Journal of Materials Chemistry C

Accepted Manuscript

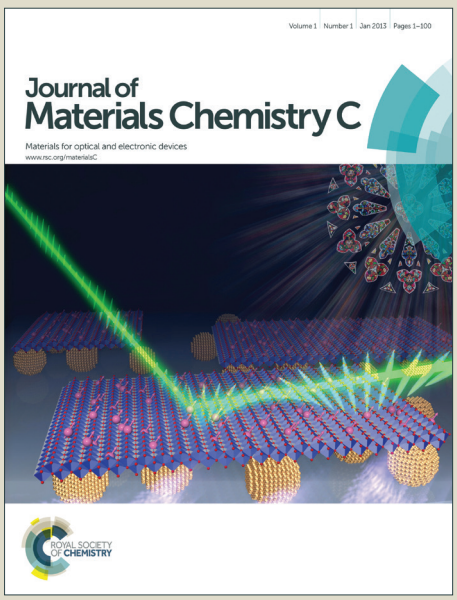

ROYAL SOCIETY OF CHEMISTRY

www.rsc.org/materialsC

Journal Name

RSCPublishing

ARTICLE

Anomalous Second Harmonic Generation (SHG) Response in $MBPO_5$ (M=Sr, Ba)

Cite this: DOI: 10.1039/x0xx00000x

Bing-Hua Lei, [a,b] Qun Jing,[a,b] Zhihua Yang,*[,a] Bingbing Zhang,[a,b] Shilie Pan*[,a]

Received 00th January 2012,
Accepted 00th January 2012

DOI: 10.1039/x0xx00000x

www.rsc.org/

Large sized ultraviolet (UV) nonlinear optical (NLO) crystals $SrBPO_5$ and $BaBPO_5$ have been obtained successfully by top-seeded solution growth method in order to study the mechanism of second harmonic generation (SHG) effect in borophosphates. Optical and thermal properties have been measured. $SrBPO_5$ and $BaBPO_5$ display large experimental gaps (6.44 and 6.14 eV) and moderate SHG coefficients (0.57 and 0.43 times of KH_2PO_4 (KDP)). More importantly, based on the further insight into the relationship between nonlinear optical properties and crystal structure within density functional theory (DFT), we discover that BO_4 groups and metal cations take essential roles in SHG effect of $MBPO_5$ (M=Sr, Ba) but not PO_4 groups as expected. Moreover, PO_4 groups play a counteractive role in $BaBPO_5$ because of indirect influence from metal cations.

Introduction

The solid state laser has many significant applications in a broad area, such as laser micromaching, semiconductor photolithography, photochemical synthesis, laser communication and so on. Owing to the ability to shorten the wavelength of light based on the process of second-harmonic generation (SHG), the nonlinear optical (NLO) crystals become the key material used in the frequency conversion device. After continuous efforts over several decades, many excellent NLO crystals were obtained. The most advanced, commercially available benchmark NLO materials for ultraviolet−visible (UV-vis) region are borates or phosphates, such as KH_2PO_4 (KDP)[1], $KTiOPO_4$ (KTP)[2, 3], β-BaB_2O_4 (BBO)[4], LiB_3O_5(LBO)[5], etc. In the last few years, many novel borate crystals and potential applications have been reported in the UV/Deep-UV region, such as $NaBeB_3O_6$[6], $K_3B_6O_{10}Cl$[7], $Cs_2B_4SiO_9$[8], $Ba_4B_{11}O_{20}F$[9] with large powder SHG responses about 1.6, 4, 4.6, 10 times of KH_2PO_4 (KDP) and short UV cutoff edges of 200, 180, 190, 175 nm, respectively. Recently, $Li_4Sr(BO_3)_2$[10] which is expected as a rival of $KBe_2BO_3F_2$ (KBBF)[11, 12], was obtained. And some phosphates such as $Ba_3P_3O_{10}Cl$[13], $Rb_2Ba_3(PO_3)_3$[14] have also drawn much attention ascribed to their short UV cutoff edges (180, 163 nm) but with weak SHG effect. Therefore, it is in urgent need of crystals with good deep UV NLO characteristics.

It is interesting to note that thanks to their complex anionic groups built of BO_4, BO_3, and PO_4 tetrahedra, borophosphates exhibit rich chemistry structure and many potential applications[15-18]. The crystal chemistry of borophosphates with anionic partial structures mainly built from tetrahedral building units reveals a large structural variety, similar to that of silicates and alum silicates. The primary BO_4, BO_3 and PO_4 building units can interconnect to form complex anionic structures from isolated species, oligomers, rings, chains, layers to framework[19]. Therefore, there is lots of room to explore novel compounds for the considerable variety in the chemical structure. For example, the $MBPO_5$ (M=Sr, Ba, Ca) compounds belong to the stillwellite structural type, and contain single chains of the BO_4 tetrahedra running parallel to [001] which are linked to terminal PO_4 tetrahedra to form spiral chains[20, 21]. BPO_4 whose structure is similar to that of silica[22] also contains BO_4 and PO_4 groups. Except for tetrahedrally coordinated B^{3+} and P^{5+}, $Co_5BP_3O_{14}$ is the first borophosphate with planar BO_3 groups connected to PO_4 tetrahedra[23]. In the respect of crystal structure, Kniep and co-workers have systematically studied borophosphate compounds in their review articles[24, 25]. Among various structures, B-O-B or B-O-P connections are observed commonly and made up of BO_3, BO_4 and PO_4 tetrahedra sharing common corners. The P-O-P connections have also been found in the borophosphates anions, such as, $Cs_2Cr_3(BP_4O_{14})(P_4O_{13})$, $CsFe(BP_3O_{11})$, $Li_2Cs_2B_2P_4O_{15}$ and $Li_3M_2BP_4O_{14}$ (M=K, Rb)[26].

Owing to the various structures of borophosphates, they exhibit different properties. Because of the absence of dangling

bonds of oxygen in BO_4 groups, several borophosphates with short UV cutoff edge have been found. There are $SrBPO_5$[20], $BaBPO_5$[21], BPO_4[27], $Sr_6BP_5O_{20}$[28], and their cutoff edges are below 185, 180, 134 and 200 nm, respectively. Unfortunately, the SHG intensities are very weak except BPO_4. It is also a common character in borophosphates or phosphates. Luckily, there are several materials with relatively large SHG responses, such as BPO_4 and $NH_4H_2PO_4$ (ADP) with the magnitude of almost double as that of KDP. In fact, for the SHG effect, the magnitude as large as that of KDP is enough for applications in UV or deep-UV wavelength[29]. Therefore, a fully understanding of the mechanism of NLO effects in borophosphate crystals can help us to design and search new excellent NLO crystals more efficiently. Generally, compared with the BO_3 group, the BO_4 group in borates is considered to have a neglectable contribution to SHG effect. While one question remains open that what the role of BO_4 is, especially in a series of borophosphates which only contain BO_4 and PO_4 anionic groups. To deeply understand their inner mechanism of NLO effects of borophosphates and then guide the design of new NLO borophosphate materials, four aspects need to be clarified: i) what the NLO-active units are, ii) how the arrangements of the NLO-active units affect macroscopic NLO effects, iii) what the relationship between NLO properties and crystal structures is, iv) how to enhance the SHG effect.

Until now, several theories have been proposed to help chemists and material scientists to design and search new NLO materials with large SHG effect. The "anionic group theory"[30], proposed by Chen et al., has proven to be successful in searching new NLO borate crystals with large SHG effects, such as BBO (5.8×KDP), LBO (about 3×KDP), etc. Besides, some materials with large SHG effect which owes to the combination of second-order Jahn-Teller units with diverse boron-oxygen functional units have emerged, typical examples are $Cd_4BiO(BO_3)_3$ (6×KDP)[31], $Pb_2B_5O_9I$ (13.5×KDP)[32]. In order to get Deep-UV NLO crystals, another rigorous prerequisite for UV/Deep-UV region is the wide transparence, which is expected to unhinder the role of NLO-active structural units. Consequently, the introduction of SOJT units usually conflicts with the short UV cutoff edge. Then, a modified bond valence sum method[33-35] has been put forward to shorten the cutoff edge. Via controlling ambient coordination environment surrounding the oxygen atoms, the band gap can be increased due to the amplitude of eliminating the nonbonding orbitals. Notable compounds are Al-containing borates: $K_2Al_2B_2O_7$ (KAB)[36], $Na_2Al_2B_2O_7$ (NABO)[37] and $Cs_2Al_2B_2O_7$ (CABO), or Be-containing borates: $Sr_2Be_2B_2O_7$ (SBBO)[38], KBBF, $MM'Be_2B_2O_6F$ (M=Na, M'=Ca; M=K, M'=Ca, Sr)[39]. Therefore, it is necessary to investigate the insight of relationship between crystal structures and NLO properties. Especially, to our best knowledge, the contribution of anionic tetrahedral groups in borophosphates for SHG still lacks investigation. Accordingly, it will be beneficial to design and search new excellent borophosphate crystals.

Herein, the isostructural compounds $SrBPO_5$ and $BaBPO_5$, which have short UV cutoff edges of 180 and 185 nm and relatively small SHG intensities of 0.439 and 0.570 KDP, were studied as a demonstration. In order to characterize their properties accurately, the $SrBPO_5$ and $BaBPO_5$ crystals were grown by the top-seeded solution method. And the additional measurements such as DTA, optical uniformity measurement, were made. Detailed investigations on the crystal structure, electronic structure and optical properties of $SrBPO_5$ and $BaBPO_5$ have been performed based on DFT calculation. To insight into the relationship between electronic structure and properties, SHG-density, band-resolved method, real-space atom-cutting method are adopted. The results of calculation agree well with those obtained from the experiments but the NLO-active units are not what we expected. Previously, if there are BO_4 and PO_4 groups in a compound, the PO_4 groups are considered to be the main contributor of SHG because borates containing BO_4 groups could possess a SHG effect smaller than that containing BO_3 groups[20, 30]. Anomalously, through precise analysis based on SHG-density and band-resolved methods, we found that the BO_4 groups and metal cations give the main contribution to SHG effect of $MBPO_5$ but not the PO_4 groups as expected. What is more, the PO_4 groups even show the counteractive contribution in $BaBPO_5$ because of indirect influence from the cations.

Experimental

Synthesis and Crystal Growth

Polycrystalline samples of $SrBPO_5$ and $BaBPO_5$ were synthesized by traditional solid-state reaction techniques. Analytically pure $SrCO_3$ (for $SrBPO_5$) or $BaCO_3$ (for $BaBPO_5$), H_3BO_3 and $NH_4H_2PO_4$ were weighted as stoichiometric ratio and mixed in an agate mortar, and then packed into a platinum crucible. After preheating at 500 °C for 20 h in muffle furnace, the mixture was cooled to ambient temperature and grinded, pressed. Then, the products were heat up to 900 °C for 72 h (for $SrBPO_5$) and 48 h (for $BaBPO_5$), and cooled to room temperature again. The results were checked by powder X-ray diffraction, and single-phase powders of $SrBPO_5$ and $BaBPO_5$ were obtained when repeated heat treatment caused no further changes in the powder X-ray diffraction pattern.

The flux method is necessary for the crystal growth of $SrBPO_5$ and $BaBPO_5$ because they are incongruently melting compounds. As they were described in previous paper[20, 21], the top-seeded solution growth method was used to grow the single crystals, BPO_4 (for $SrBPO_5$) and $Li_4P_2O_7$ ($BaBPO_5$) was used as the fluxes. The crystals were then obtained after drawn out of the solution surface, cooled to room temperature at a gradient of 20 °C/h, then slowly taken out from the furnace.

Powder X-ray Diffraction

A Bruker D2 ADVANCE X-ray diffract meter equipped with a monochromatic Cu Kα radiation (λ = 1.5418 Å) was used to measure the powder X-Ray Diffraction. The angular range from 10° to 70° (2θ) was recorded, with a scan step width of 0.02°

and a rate of 10 s step^{-1}. Theoretical simulation was conducted on the basis of the single crystal crystallographic data. The powder X-ray diffraction patterns of $SrBPO_5$ and $BaBPO_5$ are shown in Figure S1.

Numerical Calculation Details and Methods

Electronic Structure and Linear Optical Properties

The first-principles calculations were performed by the CASTEP[40], a plane-wave pseudopotential package based on the DFT. During the calculation, geometry optimization was performed using the BFGS minimization technique. The geometry optimization was converged criterion that the residual forces on the atoms were less than 0.01 eV/Å, the displacements of atoms were less than 5×10^{-4} Å, and the energy change was less than 5.0×10^{-6} eV/atom. After a series of successful tests, the exchange-correlation functional we chose was the generalized gradient approximation (GGA) with Perdew-Burke-Ernzerhof (PBE) functional. The norm-conserving pseudopotential (NCP) was used, the valence electrons were Sr-$4s^24p^65s^2$, B-$2s^22p^1$, O-$2s^22p^4$, and P-$2s^22p^3$ respectively. The energy cutoff of plane wave's basis set was 830 eV, and the Brillouin zone was composed of 4 × 4 × 4 Monkhorst-Pack k-point sampling with a separation of 0.04 Å^{-1}. We kept the default values of the CASTEP code on the aspect of the other calculation parameters and convergent criteria. The properties of $BaBPO_5$ were calculated in the same condition except for the valence electrons of Ba-$5s^25p^66s^2$.

"Scissors" correction approximation was implemented by moving all of the conduction bands off valence band with the gap correction Δ (the difference between calculated bang gap and experimental one). In the scissors operator[41-43], the momentum matrix elements should be modified. The correlative renormalization of the moment matrix elements under the gap correction is satisfied:[44]

$$P_{nm} \rightarrow \mathrm{P}_{nm}\,(\omega_{\mathrm{nm}} + \Delta/\hbar(\delta_{\mathrm{nc}} - \delta_{\mathrm{mc}}))/\omega_{\mathrm{nm}}$$

Here, $(\delta_{nc}-\delta_{mc})$ is the gap correction of the couples of bands between one valence and one conduction band state. In this process, as the GGA wave functions approach the true quasiparticle wave function[45, 46], there is a hypothesis that the $\mathbf{r}_{mn}$ mnmatrix elements is invariant.

Methology for Probing SHG Contribution from Electronic States

The so-called length-gauge formalism derived by Aversa and Sipe[47] was adopted. At a zero frequency, the static second-order nonlinear susceptibilities can be ascribed to Virtual-Hole (VH), Virtual-Electron (VE) and Two-Band (TB) processes[48].

$$\chi_{\alpha\beta\gamma}^{(2)} = \chi_{\alpha\beta\gamma}^{(2)}(\mathrm{VE}) + \chi_{\alpha\beta\gamma}^{(2)}(\mathrm{VH}) + \chi_{\alpha\beta\gamma}^{(2)}(\text{two-bands}) \quad (1)$$

Where $\chi_{\alpha\beta\gamma}^{(2)}$(VE), $\chi_{\alpha\beta\gamma}^{(2)}$(VH), and $\chi_{\alpha\beta\gamma}^{(2)}$(two bands) are computed with the formulas as follows:

$$\chi_{\alpha\beta\gamma}^{(2)}(VE) = \frac{e^3}{2\hbar m^3}\sum_{vcc'}\int\frac{d^3k}{4\pi^3}P(\alpha\beta\gamma)\,\mathrm{Im}\left[P_{cv}^{\alpha}P_{cc'}^{\beta}P_{c'v}^{\gamma}\right]\left(\frac{1}{\omega_{cv}^3\omega_{vc'}^2}+\frac{2}{\omega_{vc}^4\omega_{c'v}}\right) \quad (2)$$

$$\chi_{\alpha\beta\gamma}^{(2)}(VH) = \frac{e^3}{2\hbar m^3}\sum_{vv'c}\int\frac{d^3k}{4\pi^3}P(\alpha\beta\gamma)\,\mathrm{Im}\left[P_{vv'}^{\alpha}P_{cv'}^{\beta}P_{cv}^{\gamma}\right]\left(\frac{1}{\omega_{cv}^3\omega_{v'c}^2}+\frac{2}{\omega_{vc}^4\omega_{cv'}}\right) \quad (3)$$

$$\chi_{\alpha\beta\gamma}^{(2)}(two-bands) = \frac{e^3}{2\hbar m^3}\sum_{vc}\int\frac{d^3k}{4\pi^3}P(\alpha\beta\gamma)\frac{\mathrm{Im}\left[P_{vc}^{\alpha}P_{cv}^{\beta}(P_{vv}^{\gamma}-P_{cc}^{\gamma})\right]}{\omega_{vc}^5} \quad (4)$$

Here, α, β, γ are Cartesian components, and v/v', c/c' denote valence bands (VBs) and conduction bands (CBs). And P(αβγ), $\hbar\omega_{ij}$ and P^{α}_{ij} refer to full permutation, the band energy difference and momentum matrix elements, respectively.

The band-resolved method, revealing the effective values of individual electronic states in SHG coefficients, comes forward to emphasize the two out of three band indices for $\chi_{\alpha\beta\gamma}^{(2)}$(VE) or $\chi_{\alpha\beta\gamma}^{(2)}$(VH) in equations (2) and (3). As a result, the SHG effect of orbital contribution is divided into occupied and unoccupied bands. Therefore, the analysis scheme exhibits the orbital contributions of total $\chi^{(2)}$ with level by level vividly. In this work, the integral contribution of the band-resolved $\chi^{(2)}$ in VE and VH processes was calculated further, which can show the integral SHG contribution of the corresponding energy region and the contribution of valence bands and conduction bands[49]. So we can use it to identify and further research the main states having contribution in a SHG process.

There is another more vivid method called SHG-density[50] which can illuminate the SHG response further in complex electronic structure we researched. The SHG-density method was performed by using the effective SHG of each occupied or unoccupied band as weighting coefficient (after normalized with total VE or VH $\chi^{(2)}$ value) to sum the probability densities of all occupied or unoccupied states. Therefore, this method ensures that quantum states which cause SHG can be shown together as these occupied or unoccupied "SHG-densities", while states irrelevant to SHG will not be shown. Therefore, the origin of SHG optical nonlinearity can be highlighted in the real space through the resulting distribution of such densities. The methods have been employed successfully to analyze the SHG origin of NLO borates $Li_nM_{n-1}B_{2n-1}O_{4n-2}$(M=Cs/Rb, n=3,4,6)[49] and $Bi_2ZnOB_2O_6$[51].

Results and Discussion

Deep Ultraviolet Transmission Spectrum

Ultraviolet cut-off edge of a NLO crystal is an important indicator of its practical application range. Two large $SrBPO_5$ and $BaBPO_5$ crystals were grown and shown in Figure 1. In order to obtain their cut-off edges accurately, the UV transmission spectra of $SrBPO_5$ and $BaBPO_5$ crystals were measured in nitrogen. From the spectra, we can see that the transparencies of the $SrBPO_5$ and $BaBPO_5$ crystals are above 80% at until 200 and 209 nm, respectively, and decreases starting from 200 and 209 nm, and reaches zero at 180 and 185 nm, respectively.

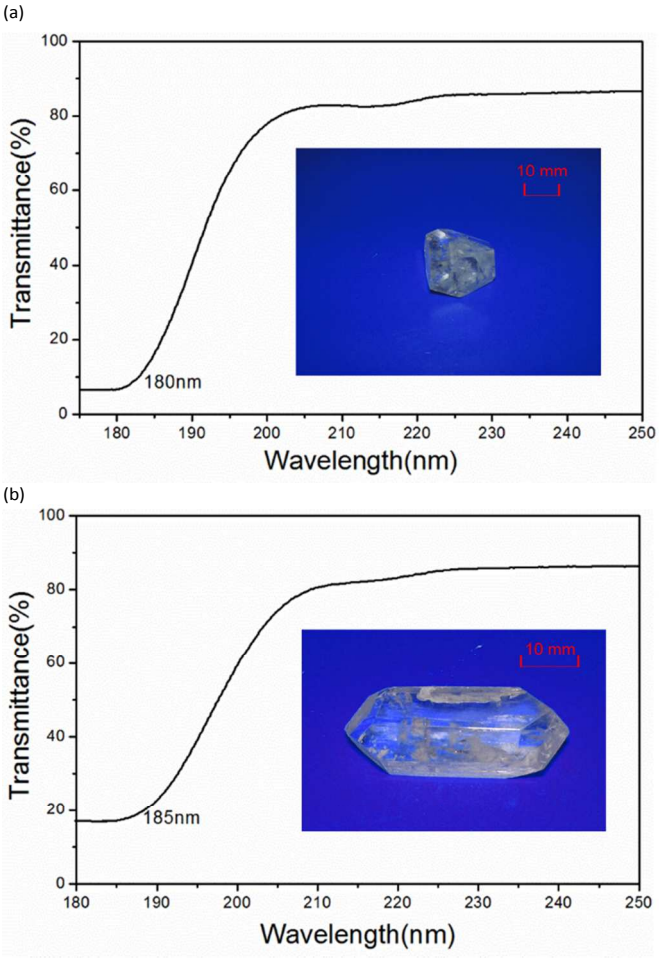

Figure 1. The ultraviolet (UV) transmission spectrum and crystal photographs of $SrBO_5$ (a) and $BaBPO_5$ (b).

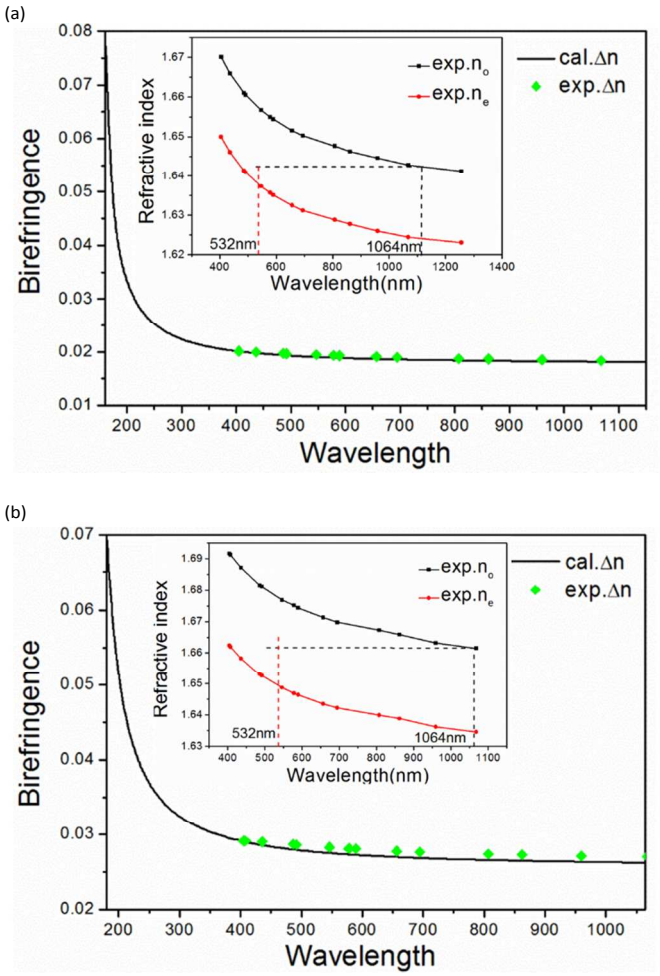

Figure 2. The calculated and experimental dispersion curves of birefringence and experimental refractive index (insert) of $SrBPO_5$ (a) and $BaBPO_5$ (b).

Birefringence and Phase Matching Curves

According to the point-group symmetry of D_3, the $SrBPO_5$ and $BaBPO_5$ crystals are uniaxial and there are only two independent nonzero diagonalizable of dielectric tensors. The uniaxial properties of them were measured by conoscope using a crystal slicing perpendicular to optical axis. Interference patterns were shown in Figure S2. The square of the refractive index **n** is equal to the real part of ε (ω). The birefringence can be obtained from the linear response functions. Figure 2 shows the calculated and experimental dispersion curves of refractive indices and birefringence. We can see that the birefringence Δn, defined as $n_o - n_e$, is about 0.018 for $SrBPO_5$ and 0.026 for $BaBPO_5$ at 1064 nm. The calculated results are consistent well with the experimental values. As shown in Figure 2, because of small dispersion of refractive indices, we can predict that $SrBPO_5$ and $BaBPO_5$ could better fulfil the phase-matching conditions.

Type I phase matching (PM) SHG curves of $SrBPO_5$ and $BaBPO_5$ were calculated according to the Sellmeier equations[20, 21] as a function of fundamental wavelength (in Figure S3). The Sellmeier equations indicate that the shortest type I PM SHG wavelengths are 395 nm for $SrBPO_5$ and 364 nm for $BaBPO_5$ respectively. Obviously, the shorted type I phase matching (PM) SHG wavelength of $BaBPO_5$ is lower than that of $SrBPO_5$.

Thermal Properties

The thermal expansion of a NLO crystal is an important factor in its growth and applications[52]. Light absorption by a crystal causes a thermal gradient that may disturb the laser oscillation, and high thermal gradients can also lead to crystal fracture. The thermal expansions of a- and c-axis of $SrBPO_5$ and $BaBPO_5$ are measured ranging 50 to 300 °C, shown in Figure 3. From this figure, the thermal expansion curves demonstrate that no anomaly within the measuring temperature range is observed and the curves are linear within this range. The average linear

thermal expansion coefficients of the a- and c-oriented in $SrBPO_5$ and $BaBPO_5$ crystals are 7.66×10^{-6} /°C, 7.81×10^{-6} /°C and 8.72×10^{-6} /°C, 7.82×10^{-6} /°C, respectively.

From the crystal structure of both compounds, one can expect that the thermal expansion coefficients of both compounds would show a small anisotropy along a- and c-axes. This is in agreement with our experimental results, thus both crystals are not cracked during the crystal growth.

The DTA curves of $SrBPO_5$ and $BaBPO_5$ were shown in Figure S4 measured from 900 to 1300 °C for $SrBPO_5$ and 900 to 1250 °C for $BaBPO_5$. As shown in the DTA curves, there are two endothermic peak at 1220 and 1238 °C for $SrBPO_5$ and two endothermic peaks at 1203 and 1121 °C for $BaBPO_5$. These results further indicate that both compounds are incongruent melting compounds. Therefore, the flux method is necessary for the purpose of their crystal growth.

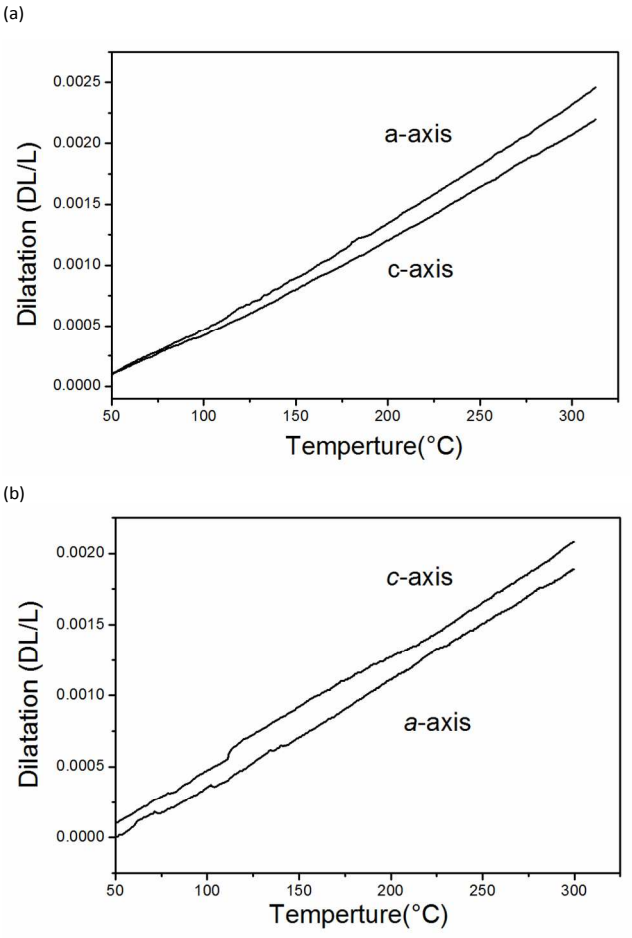

Figure 3. The thermal expansions of *a*- and *c*-axis of $SrBPO_5$ (a) and $BaBPO_5$ (b).

Optical Uniformity Measurement

Optical homogeneity of the crystal (Figure S5) is also an important indicator of practical application. Therefore, a single crystal with a size of 3.50 × 3.50 × 3.45 mm^3 of $SrBPO_5$ and a size of 3.50 × 3.50 × 3.45 mm^3 of $BaBPO_5$ with a laser of wavelength of 632.8 nm were measured in this experiment. The values of optical uniformity are 1.26×10^{-5} /cm ($SrBPO_5$) and 2.48×10^{-5} /cm ($BaBPO_5$), which indicates that both crystals have high qualities.

Electronic Structure

The band structures of $SrBPO_5$ and $BaBPO_5$ are also very similar. $SrBPO_5$ and $BaBPO_5$ are direct gap (Figure S6) crystals with the calculated band gaps of 6.15 and 5.89 eV, as shown in Table 1. Comparing with the optical experimental gaps 6.44 ($SrBPO_5$) and 6.14 eV ($BaBPO_5$), the calculated gaps were in agreement very well. And the very small difference between the calculated and the experimental ones is because of the discontinuity of exchange-correlation energy. To get linear and NLO optical properties more accurately, we need the resonances occurring at the correct energies. The scissors operator will be applied to the computation of optical properties.

Figure 4 shows the partial density of states (PDOS) of $SrBPO_5$ and $BaBPO_5$. For $SrBPO_5$, the main occupant is O-2p orbital in the VBs near the Fermi surface and the Sr-4p orbitals at the bottom of the CBs, which suggests that the Sr-O bonds determine the band gap. Differently, in $BaBPO_5$, Ba-5d orbital is dominant at the bottom of CBs. It means that the Ba-O bond controls the band gap of $BaBPO_5$. Therefore the difference between electronic structures of Sr and Ba makes a red shift about 0.17 eV for $BaBPO_5$ comparing with $SrBPO_5$.

Table 1. The calculated and experimental band gaps of $SrBPO_5$ and $BaBPO_5$.

Crystal	Calcd.	Expel.	Difference
$SrBPO_5$ (eV)	6.15	6.44	0.29
$BaBPO_5$ (eV)	5.98	6.14	0.16

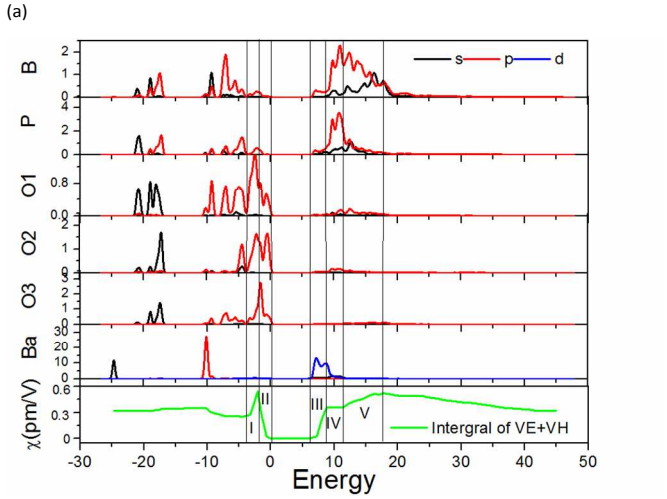

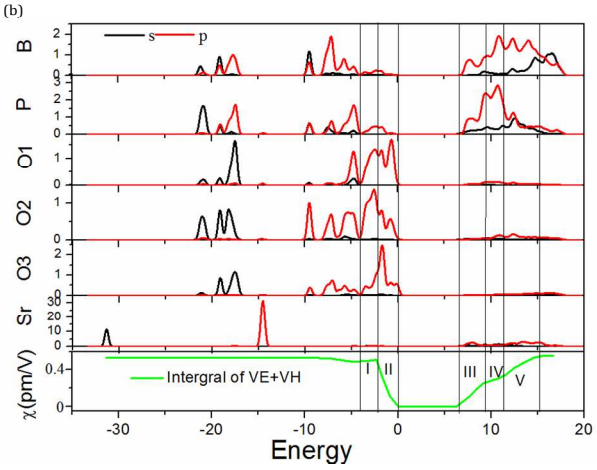

Figure 4. The PDOS of $SrBPO_5$ (a) and $BaBPO_5$ (b). I-V regions refer to the negative contribution region, the main contribution region in VBs, the main contribution region in CBs, the offset contribution to the SHG coefficient, the second contribution in CBs.

NLO Properties

We calculated SHG coefficients d_{ij} under the static limit within the length gauge. According to the D_3 point-group symmetry and Kleinman symmetry, only d_{11} should be determined. The experimental SHG intensities and computed ones at combinations of exchange-correlation functional and pseudopotentials are shown in Table 2. The result, calculated on the condition of GGA and NCP, agrees well with the experimental result, which proves the validity of our studies on $SrBPO_5$ and $BaBPO_5$ with the GGA plane-wave pseudopotential method.

Table 2. Comparisons of the calculated SHG coefficients with a correction of the band gap and experimental SHG effect of $SrBPO_5$ and $BaBPO_5$.

Crystal	Expel.	Calcd. d_{11}(pm/V)	VE	VH
$SrBPO_5$	0.57KDP	0.218(0.56KDP)	0.268	-0.05
$BaBPO_5$	0.43KDP	0.157(0.40KDP)	0.137	0.02

SHG Response in $MBPO_5$

Distribution of the Electron States to SHG Response

For the process of NLO effects, the short-range forces rather than long-range interactions play a decisive role. In other words, in the NLO effects, the electron motion may be regarded as confined to small regions and any NLO susceptibility (or second-order susceptibility) in crystals is a localized effect arising from the action of incident photons on the electrons in certain orbitals of atomic clusters[30]. In this work, to study the distribution of the electron states in SHG response, the integral contribution[49] of the band-resolved $\chi^{(2)}$ in VE and VH processes and the SHG-density were calculated.

Figure 4 shows the partial density of states (PDOS) and integral of band-resolved $\chi^{(2)}$ of $SrBPO_5$ and $BaBPO_5$, which counts the integral contribution of SHG effect in the energy representation. Here we choose $BaBPO_5$ as a demonstration to locate certain orbital of atomic clusters using the band-resolved method. According to the variation of integral of band-resolved $\chi^{(2)}$ (green curves in Figure 4), the PDOS was divided into several regions in energy. In the region I (-3.81 eV~ -2.01 eV) in Figure 4a, the electrons of O1-p_z (the nonbonding p orbital) and the bonding orbital of O2 occupy this energy region and the integral of band-resolved $\chi^{(2)}$ decrease, which suggests that the contribution of this region is negative. Meanwhile, the electrons of the nonbonding p orbital of O2 and O3 atom occupy the region II (-2.01~0.00 eV), and the integral of band-resolved $\chi^{(2)}$ increases which corresponds to positive contributions to SHG effect. Similarly, in the region III (6.3~8.6 eV), the most part is Ba-5d orbital and it is the main positive contribution in CBs according to the curve of integral of band-resolved $\chi^{(2)}$.

Except for the contribution of electronic states within energy band framework, the electronic structure subsystem which causes SHG can be visualized via the SHG-density method. According to the results shown in Table 2, the VE process would be analysed due to its domination in the SHG response in $BaBPO_5$. Interestingly, different microscopic groups or atoms exhibit different contributions: the PO_4 groups give a negative contribution (Figure 5a) to SHG effect, while the BO_4 groups and metal cations own positive contributions (Figures 6b-6d). To clarify such counteraction from different parts, we studied the main contribution region and corresponding orbitals in energy. Figure 5a shows the counteractive contributor in the region I which corresponds to 2p orbitals of oxygen in PO_4. We can see that orbital and negative SHG density have a great overlap. In other words, the p-electron orbital of oxygen in PO_4 groups, which play the counteractive role of SHG effect. Oppositely, we can see the positive contributions which come from the BO_4 groups and are corresponding to p orbitals of O3 in Figure 5b. Figure 5c shows the contribution of the region III (6.3 eV~8.6 eV). The SHG density sprinkles on Ba-5d orbital but not on the B-2p and P-3p orbital, which indicates that the Ba-5d orbital is the main contributor in this region. Similarly, in the region V, the anti-**σ** orbital of the B-O bond is the main contributor in SHG density, which illustrates the importance of BO_4 groups as shown in Figure 5d. In conclusion, the PO_4 groups have negative contributions while the BO_4 groups and the Ba metal cations are the main contributors to SHG effect of $BaBPO_5$.

The same methology was employed to analyze the SHG response of $SrBPO_5$. The main difference from $BaBPO_5$ is that the counteraction contributions almost vanish in the region I. Meanwhile, we can find the same SHG response of BO_4 like Figure 5c in $SrBPO_5$ in region III, IV and V and this response has not been observed in PO_4. That is to say, the BO_4 group is still the main contributor of SHG effect. In addition, compared the region III of $SrBPO_5$ and $BaBPO_5$ in Figure 4, owing to the absence of d orbital of the Sr atom (Figure 4b), the DOS of the B atom and the P atom increases. This change is bound to

whittle the contribution of metal cations and strengthen the contribution of BO_4. This phenomenon will be further confirmed by the real-space atom-cutting method in the next section. Therefore, the BO_4 groups become the main role in SHG effect of $SrBPO_5$.

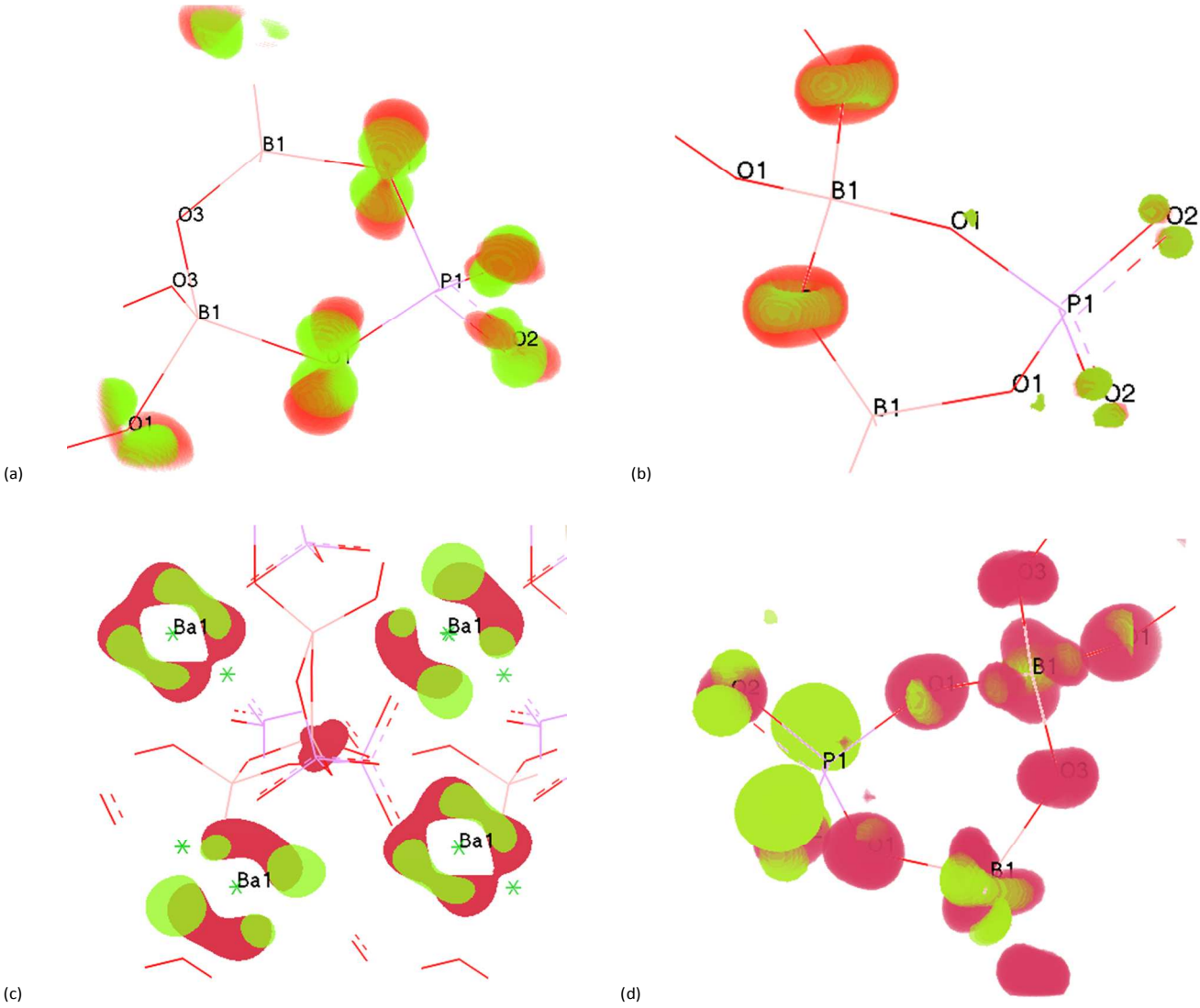

Figure 5. The SHE-density of VE process for $BaBPO_5$. (a) The negative contribution in SHG density of occupied states (orange) and the corresponding orbitals (green), (b) The positive contribution in SHG density of occupied states (orange) and the corresponding orbitals (green), (c) The positive contribution of unoccupied states (red) of Ba and the corresponding orbitals (green), (d) the positive contribution of unoccupied states (red) of BO_4 and the corresponding orbitals (green).

The Significance of *d* Orbital

Although we found the main contribution of SHG effect in $MBPO_5$, there is still one question: why the counteractive contribution vanishes in $SrBPO_5$. In the matter of crystal structure, $SrBPO_5$ and $BaBPO_5$ are isostructural and possess similar lattice parameters: a=7.12 Å, c=6.96 Å and a=6.84 Å, c=6.79 Å, respectively. The bond lengths and angles of BO_4 and PO_4 are almost the same. The radii of Ba and Sr atom are 2.78 Å and 2.45 Å. The radius difference of cation may cause the local distortion of the polyhedral and overall framework structures in some compounds such as $ACuTe_2O_7$ (A = Sr2+,Ba2+,or Pb^{2+})[53], $ANaNbOF_5$ (A=K, Cs)[54], $AMoO_3(IO_3)$(A=K, Rb, Cs)[55], $AGa(SeO_3)_2$(A = Li, Na, K, and Cs)[56], $A_2Ti(IO_3)_6$(A=Li, Na, K, Rb, Cs, Tl)[57] and $MM'Be_2B_2O_6F$ (M=Na, M'=Ca; M=K, M'=Ca, Sr)[58]. In this work, we employed Gaussian[59] to calculate the dipole moments of MO polyhedra and the result suggests that there is no difference in $SrBPO_5$ and $BaBPO_5$. Therefore, we think that the radius difference of cation will not cause the local distortion of the tetrahedral and overall framework structures and also cannot cause different SHG effect of metal and PO_4 group. In fact, the dangling bond of the terminal oxygen exists only in PO_4 and is easily influenced by the metal cations, which means that metal cations make great difference to PO_4 rather than BO_4.

The influence of the metal cations to the terminal oxygen (O2 for $BaBPO_5$ and O1 for $SrBPO_5$) and boron-phosphorus bridge oxygen (O1 for $BaBPO_5$ and O2 for $SrBPO_5$) in PO_4 can be reflected in the lowest unoccupied molecular orbital (LUMO, Figure 6). It is noted that the interaction between terminal oxygen or boron-phosphorus bridge oxygen in PO_4 and metal cation is stronger than that between boron-boron bridge oxygen O3 in BO_4 and metal cation. More importantly, the electronic structure and PDOS show that *d* orbitals of the Ba cations dominate in LUMO, while B and P dominate in LUMO in $SrBPO_5$. This suggests that, the interaction between oxygens and Ba cations in $BaBPO_5$ is stronger than that in $SrBPO_5$. Thus, the Ba-5d orbital is closely related to the properties of PO_4. And owing to the absence of *d* orbital of Sr, the counteractive contribution from PO_4 vanishes in $SrBPO_5$. There is no wonder that the contribution of PO_4 in SHG effect in $SrBPO_5$ and $BaBPO_5$ are different. Meanwhile, the Ba cations because of their *d* orbitals have more contribution in SHG effect in $BaBPO_5$.

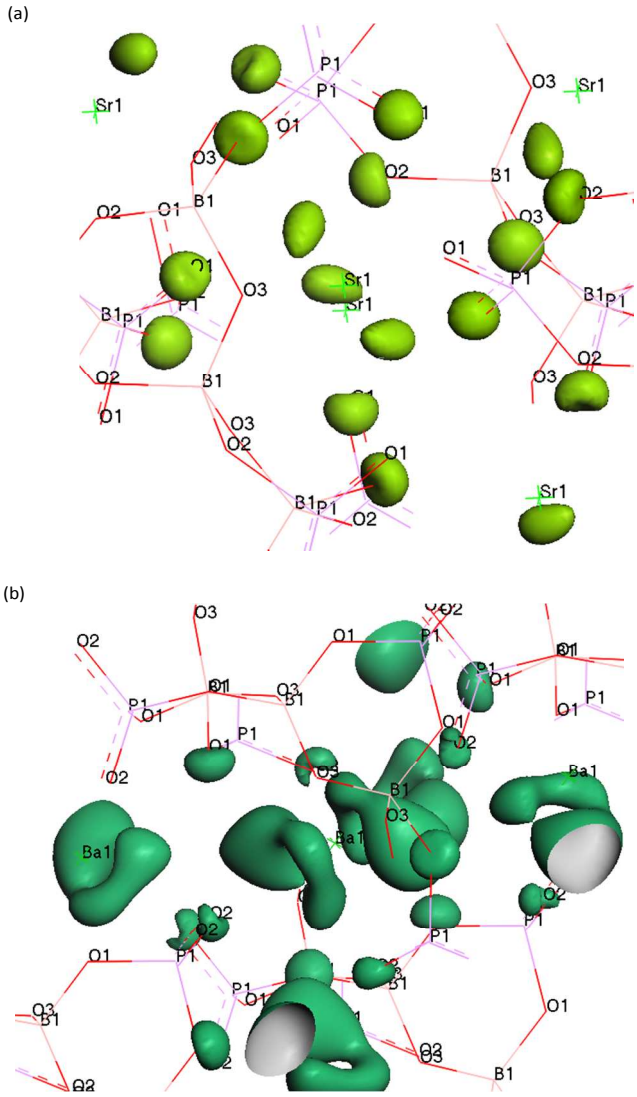

Figure 6. The LUMO of $SrBPO_5$ (a) and $BaBPO_5$ (b).

Spatial Contributions of Groups and Ions to SHG Response

Strangely enough, it is believed previously that if there are PO_4 and BO_4 together, the PO_4 group should be the main contributor to the SHG effect[20]. Perhaps they do not take microstructure into consideration. In order to verify the contribution of Ba and BO_4 groups and the counteractive of PO_4, the real-space atom-cutting method[51] was employed in our work. In the "cutting", it is of importance to determine the suitable cutting radii of Ba, B, P and O1-O3. Owing to the charge-density distributions and the overlap behaviours in these compounds, the cutting radii of Sr, Ba, B, P, O are 1.80 , 1.80, 0.82, 1.52, 1.11 Å, respectively. According to Rietveld technique, for $BaBPO_5$, the anionic groups are BO_4 and PO_4, not BPO_7[60] and its decomposed products are $Ba_3BP_3O_{12}$ and $Ba_2P_2O_7$. Hence, BO_4 or PO_4 can be regarded as a group to be cut and the bridge oxygen is assigned to PO_4 group because it has stronger interaction with phosphorus than boron according to the decomposed products. Consequently, the contributions are: d_{11}(Ba) = -0.11 pm/V, d_{11} (PO_4) = 0.20 pm/V, d_{11}(BO_4) = -0.26 pm/V. It is worth noting that the total value of d_{11} of $BaBPO_5$ is negative (For convenience, we convert the value of d_{11} to positive in the band-resolved analysis of Figure 4 and Table 2). So the contribution of PO_4 is counteractive. The cutting results of $SrBPO_5$ are as expected: d_{11}(PO_4) = 0.03 pm/V, d_{11}(BO_4) = 0.20 pm/V, d_{11}(Sr) = 0.04 pm/V. Consequently, in $SrBPO_5$, the PO_4 groups have a very tiny contribution.

The results obtained from the real-space atom-cutting method confirm the contributions of different groups or ions. The curious effect from the metal cations is revealed further: i) direct contribution from the Ba ions is more apparent than that from the Sr ions, which is due to the difference from the electron states; ii) indirect influence from metal cations to the BO_4 and PO_4 groups leads to dominant action of BO_4 in both crystals, and a counteractive contribution of the PO_4 groups in $BaBPO_5$ but a positively tiny contribution in $SrBPO_5$.

Conclusions

In summary, electronic structure and optical properties of $MBPO_5$ were studied theoretically and experimentally. The large crystal of $SrBPO_5$ and $BaBPO_5$ have been successfully grown by top-seeded solution growth method. Additional measurements, such as optical uniformity and thermal expansion measurements, were made. The results demonstrate that $SrBPO_5$ and $BaBPO_5$ have good optical qualities. We employed the band-resolved method, SHG-density method, real-space atom-cutting method and band-resolved method to analyze the NLO properties. The result suggests that the main contribution of SHG in $BaBPO_5$ is BO_4 and the Ba cations while the main NLO-active units in $SrBPO_5$ are almost BO_4 groups. Fallaciously, the PO_4 groups do not undertake the main role. On the contrary, it has the counteractive effect in $BaBPO_5$. Remarkably, through analysing the mechanism of the origin of

SHG effects in $MBPO_5$, we find that apart from BO_4 and PO_4, metal cations such as Ba in $BaBPO_5$ may have an important role in SHG effect. In addition, although BO_4 and PO_4 can be regarded as the NLO-active contribution candidates, whether they could make contribution in the SHG responses depends on the coordination environments and also the cations.

In addition, from this work, we can see that the contribution of the BO_4 groups and metal cations to SHG effect in some cases should not be ignorable, which may enlighten the design and search of new excellent NLO crystals. Taking $BaBPO_5$ as the example, if the PO_4 groups do not exhibit counteractive contribution to SHG effect, the SHG effect of $BaBPO_5$ will be about as large as that of KDP. Hence, a full understanding of the mechanism of NLO effects can be helpful to design and search new excellent NLO crystals.

Acknowledgment

This work is supported by National Basic Research Program of China (Grant Nos. 2014CB648400, 2012CB626803), "Western Light Joint Scholar Foundation" Program of CAS (Grant No. LHXZ201101), the National Natural Science Foundation of China (Grant Nos. 11474353, U1129301, 11104344), the Recruitment Program of Global Experts (1000 Talent Plan, Xinjiang Special Program), Major Program of Xinjiang Uygur Autonomous Region of China during the 12th Five-Year Plan Period (Grant No. 201130111), the Funds for Creative Cross & Cooperation Teams of CAS, Xinjiang International Science & Technology Cooperation Program (20146001).

Notes and references

[a] Key Laboratory of Functional Materials and Devices for Special Environments of CAS; Xinjiang Key Laboratory of Electronic Information Materials and Devices, Xinjiang Technical Institute of Physics and Chemistry of CAS, Urumqi 830011, China. Fax: (86)-991-3838957; Tel: (86)-991-3810816; E-mail: zhyang@ms.xjb.ac.cn (Zhihua Yang); slpan@ms.xjb.ac.cn (Shilie Pan),

[b] University of Chinese Academy of Sciences, Beijing 100049, China

1. J. J. De Yoreo, A. K. Burnham and P. K. Whitman, *Int. Mater. Rev.*, 2002, **47**, 113.
2. V. G. Dimitriev, *Springer: Berlin*, 1991.
3. A. H. Reshak, I. V. Kityk and S. Auluck, *J. Phys. Chem. B*, 2010, **114**, 16705.
4. C. T. Chen, B. Wu, A. Jiang and G. You, *Sci. Sin. Ser. B*, 1985, **28**, 235.
5. C. T. Chen, Y. C. Wu, A. D. Jiang, B. C. Wu, G. M. You, R. K. Li and S. J. Lin, *J. Opt. Soc. Am. B*, 1989, **6**, 616.
6. S. C. Wang, N. Ye, W. Li and D. Zhao, *J. Am. Chem. Soc.*, 2010, **132**, 8779.
7. H. Wu, S. Pan, K. R. Poeppelmeier, H. Li, D. Jia, Z. Chen, X. Fan, Y. Yang, J. M. Rondinelli and H. Luo, *J. Am. Chem. Soc.*, 2011, **133**, 7786.
8. H. Wu, H. Yu, S. Pan, Z. Huang, Z. Yang, X. Su and K. R. Poeppelmeier, *Angew. Chem. Int. Ed.*, 2013, **52**, 3406.
9. H. Wu, H. Yu, Z. Yang, X. Hou, X. Su, S. Pan, K. R. Poeppelmeier and J. M. Rondinelli, *J. Am. Chem. Soc.*, 2013, **135**, 4215.
10. S. Zhao, P. Gong, L. Bai, X. Xu, S. Zhang, Z. Sun, Z. Lin, M. Hong, C. Chen and J. Luo, *Nat. Commun*, 2014, **5**, 4019.
11. C. T. Chen, Z. Y. Xu, D. Q. Deng, J. Zhang, G. K. L. Wong, B. C. Wu, N. Ye and D. Y. Tang, *Phys. Rev. Lett.*, 1996, **68**, 2930.
12. C. T. Chen, N. Ye, J. Lin, J. Jiang, W. Zeng and B. Wu, *Adv. Mater.*, 1999, **11**, 1071.
13. P. Yu, L. M. Wu, L. J. Zhou and L. Chen, *J. Am. Chem. Soc.*, 2014, **136**, 480.
14. S. Zhao, P. Gong, S. Luo, L. Bai, Z. Lin, C. Ji, T. Chen, M. Hong and J. Luo, *J. Am. Chem. Soc.*, 2014, **136**, 8560.
15. R. Kniep, *Angew. Chem. Int. Ed.*, 1994, **106**, 791.
16. R. Kniep, *Angew. Chem. Int. Ed.*, 1999, 3857.
17. T. Yang, J.-L. Sun, G.-B. Li and L.Eriksson, *Chem. Eur. J.*, 2008, **14**, 7212.
18. D.Zhao, W.-D. Cheng, H. Zhang, S.-P. Huang and Z. Xie, *Inorg. Chem.*, 2009, **48**, 6623.
19. R. Kniep, H. Engelhardt and C. Hauf, *Chem. Mater.*, 1998, **10**, 2930.
20. S. Pan, Y. Wu, P. Fu, G. Zhang, Z. Li, C. Du and C. T. Chen, *Chem. Mater.*, 2003, **15**, 2218.
21. S. Pan, Y. Wu, P. Fu, X. a. Wang, G. Zhang and C. T. Chen, *J. Opt. Soc. Am. B*, 2004, **21**, 761.
22. Zhihua Li, Z. Lin, Y. Wu, P. Fu, Z. Wang and C. Chen, *Chem. Mater.*, 2004, **16**, 2906.
23. R. P. Bontchev and S. C. Sevov, *Inorg. Chem.*, 1996, **35**, 6910.
24. B. Ewald, Y.-X. Huang and R. Kniep, *Z. Anorg. Allg. Chem.*, 2007, **633**, 1517.
25. R. Kniep, H. Engelhardt and C. Hauf, *Chem. Mater.*, 1998, **10**, 2930.
26. Y. Wang, S. Pan and Y. Shi, *Chem. Eur. J.*, 2012, **18**, 12046.
27. X. Zhang, L. Wang, S. Zhang, G. Wang, S. Zhao, Y. Zhu, Y. Wu and C. Chen, *J. Opt. Soc. Am. B*, 2011, **18**, 2236.
28. H. Ehrenberg, S. Laubach, P. C. Schmidt, R. McSweeney, M. Knapp and K. C. Mishra, *J. Solid State Chem.*, 2006, **179**, 968.
29. W. Yao, R. He, X. Wang, Z. Lin and C. Chen, *Adv. Opt. Mat.*, 2014, **2**, 411.
30. C. T. Chen, Y. Wu and R. Li, *Int. Rev. In Phys. Chem*, 1989, **8**, 65.
31. W.-L. Zhang, W.-D. Cheng, H. Zhang, L. Geng, C.-S. Lin and Z.-Z. He, *J. Am. Chem. Soc.*, 2010, **132**, 1508.
32. Y.-Z. Huang, L.-M. Wu, X.-T. Wu, L.-H. Li, L. Chen and Y.-F. Zhang, *J. Am. Chem. Soc.*, 2010, **132**, 12788.
33. R. He, Z. S. Lin, T. Zheng, H. Huang and C. T. Chen, *J Phys Condens Matter*, 2012, **24**, 145503.
34. L. Kang, Z. Lin, J. Qin and C. Chen, *Sci Rep*, 2013, **3**, 1366.
35. R. He, H. Huang, L. Kang, W. Yao, X. Jiang, Z. Lin, J. Qin and C. Chen, *Appl. Phys. Lett.*, 2013, **102**, 231904.
36. Z. G. Hu, T. Higashiyama, M. Yoshimura, Y. K. Yap, Y. Mori and T. Sasaki, *Jpn. J. Appl. Phys.*, 1998, **37**, L1093.
37. M. He, L. Kienle, A. Simon, X. L. Chen and V. Duppel, *J. Solid State Chem.*, 2004, **177**, 3212.
38. C. T. Chen, Y. B. Wang, B. C. Wu, K. Wu, W. L. Zeng and L. H. Yu, *Nature*, 1995, **373**, 322.
39. H. W. Huang, J. Y. Yao, Z. H. Lin, X. Y. Wang, W. J. Yao, N. X. Zhai, C. T. Chen and R. He, *Chem. Mater.*, 2011, **23**, 5457.
40. S. J. Clark, M. D. Segall, C. J. Pickard, P. J. Hasnip, M. J. Probert, K. Rrfson and M. C. Payne, *Z. Kristallogr.*, 2005, **220**, 567.
41. R. W. Godby, M. Schluter and L. J. Sham, *Phys. Rev. B*, 1988, **37**, 10159.
42. C. S. Wang and B. M. Klein, *Phys. Rev. B*, 1981, **24**, 3417.
43. M. S. Hybertsen and S. G. Louie, *Phys. Rev. B*, 1986, **24**, 5390.
44. S. N. Rashkeev, W. R. L. Lambrecht and B. Segall, *Phys. Rev. B*, 1998, **57**, 3905.
45. R. W. Godby, M. Schlueter and L. J. Sham, *Phys. Rev. B*, 1988, **37**, 10159.
46. O. Gunnarsson and K. Schoenhammer, *Phys. Rev. Lett.*, 1986, **56**, 1968.
47. C. Aversa and J. E. Sipe, *Phys. Rev. B*, 1995, **52**, 14636.

48. J. Lin, M.-H. Lee, Z.-P. Liu, C. J. Pickard and C. Chen, *Phys. Rev. B*, 1999, **60**, 13380.
49. B. Zhang, Z. Yang, Y. Yang, M.-H. Lee, S. Pan, Q. Jing and X. Su, *J. Mater. Chem. C*, 2014, **2**, 4133.
50. C.-h. Lo, M. D. thesis and T. University, 2005.
51. X. Su, Y. Wang, Z. Yang, X.-C. Huang, S. Pan, F. Li and M.-H. Lee, *J. Phys. Chem. C* 2013, **117**, 14149.
52. W. B. Hou, D. Xu, D. R. Yuan, M. G. Liu, N. Zhang, X. T. Tao, S. Y. Sun and M. H. Jiang, *Cryst. Res. Technol.*, 1994, **29**, 939.
53. J. Yeon, S. H. Kim, M. A. Hayward and P. S. Halasyamani, *Inorg. Chem.*, 2011, **50**, 8663.
54. M. R. Marvel, J. Lesage, J. Baek, P. S. Halasyamani, C. L. Stern and K. R. Poeppelmeier, *J. Am. Chem. Soc.*, 2007, **129**, 13963.
55. R. E. Sykora, K. M. Ok, P. S. Halasyamani and T. E. Albrecht-Schmitt, *J. Am. Chem. Soc.*, 2002, **124**, 9.
56. D. W. Lee and K. M. Ok, *Inorg. Chem.*, 2013, **52**, 5176.
57. H.-Y. Chang, S.-H. Kim, K. M. Ok and P. S. Halasyamani, *J. Am. Chem. Soc.*, 2009, **131**, 6865.
58. H. Huang, J. Yao, Z. Lin, X. Wang, R. He, W. Yao, N. Zhai and C. Chen, *Chem. Mat.*, 2011, **23**, 5457.
59. Gaussian 09, Revision C.01, M. J. Frisch, G. W. Trucks, H. B. Schlegel, G. E. Scuseria, M. A. Robb, J. R. Cheeseman, G. Scalmani, V. Barone, B. Mennucci, G. A. Petersson, H. Nakatsuji, M. Caricato, X. Li, H. P. Hratchian, A. F. Izmaylov, G. Z. J. Bloino, J. L. Sonnenberg, M. Hada, M. Ehara, K. Toyota, R. Fukuda, J. Hasegawa, M. Ishida, T. Nakajima, Y. Honda, O. Kitao, H. Nakai, T. Vreven, J. A. Montgomery, J. E. Peralta, F. Ogliaro, M. Bearpark, J. J. Heyd, E. Brothers, K. N. Kudin, V. N. Staroverov, R. Kobayashi, J. Normand, K. Raghavachari, A. Rendell, J. C. Burant, S. S. Iyengar, J. Tomasi, M. Cossi, N. Rega, J. M. Millam, M. Klene, J. E. Knox, J. B. Cross, V. Bakken, C. Adamo, J. Jaramillo, R. Gomperts, R. E. Stratmann, O. Yazyev, A. J. Austin, R. Cammi, C. Pomelli, J. W. Ochterski, R. L. Martin, K. Morokuma, V. G. Zakrzewski, G. A. Voth, P. Salvador, J. J. Dannenberg, S. Dapprich, A. D. Daniels, ¨ O. Farkas, J. B. Foresman, J. V. Ortiz, J. Cioslowski and G. I. D. J. Fox, Wallingford CT,, 2009.
60. Y. Shi, J. Liang, H. Zhang, Q. Liu, X. Chen, J. Yang, W. Zhuang and G. Rao, *J. Solid State Chem.*, 1998, **135**, 43.

Table of Contents graphic

Anomalous Second Harmonic Generation (SHG) Response in $MBPO_5$ (M=Sr, Ba)

Bing-Hua Lei, [a,b] Qun Jing,[a,b] Zhihua Yang,*,[a] Bingbing Zhang,[a,b] Shilie Pan*,[a]

[a] Key Laboratory of Functional Materials and Devices for Special Environments of CAS; Xinjiang Key Laboratory of Electronic Information Materials and Devices, Xinjiang Technical Institute of Physics and Chemistry of CAS, Urumqi 830011, China. Fax: (86)-991-3838957; Tel: (86)-991-3810816;

[b] University of Chinese Academy of Sciences, Beijing 100049, China

*E-mail: zhyang@ms.xjb.ac.cn, slpan@ms.xjb.ac.cn

Tel: (86)-991-3810816

Fax: (86)-991-3838957

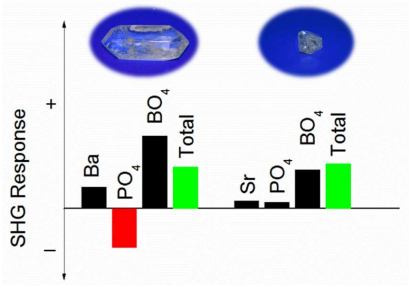

Based on SHG-density and band-resolve analysis, we find that BO_4 groups and metal cation are the main contribution in SHG effect of $MBPO_5$ (M=Ba, Sr) but not the PO_4 groups as previously expected.